Chemical Engineering Journal 306 (2016) 942–952

Contents lists available at ScienceDirect

Chemical Engineering Journal

journal homepage: www.elsevier.com/locate/cej

Photocatalytic coating for indoor air purification: Synergetic effect of photocatalyst dosage and silica modification

S. Lorencik [a,b], Q.L. Yu [a,*], H.J.H. Brouwers [a,c]

[a] Department of the Built Environment, Eindhoven University of Technology, P.O. Box 513, 5600MB, Eindhoven, The Netherlands
[b] Materials Innovation Institute, Mekelweg 2, 2600 GA, Delft, The Netherlands
[c] State Key Lab of Silicate Materials for Architectures, Wuhan University of Technology, Wuhan 430070, PR China

HIGHLIGHTS

- A photocatalytically active coating was designed and characterized.
- A pre-treatment method for photocatalytic promotion was evaluated.
- The developed coatings show high photocatalytic efficiency.
- Nano-silica modification enhances photocatalytic efficiency under visible light.
- Photocatalytic reaction rate and reactive uptake coefficient were calculated.

ARTICLE INFO

Article history:
Received 1 June 2016
Received in revised form 23 July 2016
Accepted 25 July 2016
Available online 27 July 2016

Keywords:
Photocatalytic coating
Indoor air quality
Nano-silica
Carbon-doped titanium dioxide
Reaction rate
Reactive uptake coefficient

ABSTRACT

The present work addresses the effect of nano-silica modification on a carbon-doped titanium dioxide (C–TiO_2) suspension for the development of a photocatalytic coating for indoor air improvement. The dosage effect of the applied coating and the effect of the ultraviolet pre-treatment, as an activation technique, on the photocatalytic efficiency were studied. A plug-flow experimental setup was employed for the photocatalytic efficiency assessment under realistic indoor air environment.

The results showed that the nano-silica addition and the UV pre-treatment enhanced the photocatalytic efficiency of the developed coatings. The nano-silica modification was more beneficial when the coatings were applied in higher photocatalyst dosages (0.84 mg·cm^{-2} or 1.27 mg·cm^{-2} of C–TiO_2) especially during the UV pre-treatment. The silica-modified samples tested under visible light and reduced flow rate of 1.5 L·min^{-1} degraded up to 65% and 78% of NO (up to 43% and 60% of NO_x) under initial concentration of 0.5 and 0.1 ppm, respectively. Moreover, the reaction rate and reactive uptake coefficient of the developed coatings were computed.

1. Introduction

The increased public concern about the environmental pollution has led to the development of effective pollutants removal technologies, which are better known as advanced oxidation processes (AOPs). Among these AOPs, a great interest is paid to photocatalytic oxidation (PCO) due to its potential to degrade a wide range of inorganic and organic pollutants in the air or in the aqueous media under ambient conditions, without significant energy demands.

Pure or modified titanium dioxide (TiO_2) has been proved to be an efficient material in degrading organic and inorganic air pollutants [1–4]. Among various TiO_2-anchoring methods, such as sol-gel, thermal treatment, chemical vapor deposition, electrodeposition, etc., the direct compounding method has been extensively considered because of its convenience in operation, comparatively low cost and suitability for massive production [5]. Nano-fillers and polymer supporters are in this case prepared separately and then mixed in a solution or emulsion form.

The development of coatings with immobilized TiO_2 is important for various applications, such as air purification or water treatment. Thin coatings appear to be a perfect economical solution, because of the low material consumption. However, thin coatings might not possess optimal properties, due to the small number of active sites, because of the lower amount of total immobilized or exposed photocatalytic material. Increasing the film thickness can, to some extent, lead to an enhanced utilization of the immo-

* Corresponding author.
E-mail address: q.yu@bwk.tue.nl (Q.L. Yu).

http://dx.doi.org/10.1016/j.cej.2016.07.093
1385-8947/

bilized photocatalytic material [6–8]. There the particle size of the immobilized TiO_2 plays a very important role [9,10].

The application of photocatalytic air treatment in indoor environment mostly gravitates towards "*active photocatalytic products*" such as ventilation system (stand-alone or incorporated into existing ones) consisting mostly of a pump or a fan, a lighting source and immobilized photocatalyst [11]. This is beneficial because of the improved mass transfer [11], since all the air is forced through the photocatalyst (e.g. by means of a photocatalytic mesh) and the possibility for an increased light intensity (even UV), which can be evenly distributed along the photocatalyst. In addition, the photocatalyst is protected against possible mechanical damage by the casing of the PCO ventilation system. The drawbacks of this application are the increased energy demand, necessity for maintenance and high risk of deactivation of the photocatalyst, because of the small active area limited by the casing of the ventilation system.

An alternative solution to this can be the application of "passive photocatalytic products", which do not require any additional form of energy or maintenance in order to purify air. A passive photocatalytic product can be, in theory, any type of surface, which is exposed to indoor air pollutants, humidity and light. Therefore, a surface top-coated with a photocatalytic coating is potentially an ideal option. Since the application of solvent-based coatings is due to the health hazards restrained [12], the water-based coatings are the most suitable solution. Some researchers studied the effect of the incorporation of TiO_2 into the coatings applied on plastics, glass, textiles or wood products [13–18]. The challenge in the incorporation of TiO_2 lies in a proper distribution of the photocatalyst, in protection of the binder, which contains mainly C–C bonds and can be degraded by the photocatalyst [10], and in exposure of the photocatalyst to the environment in order to work [19]. Surface modifications of the TiO_2, in order to improve some of the abovementioned properties are reported in the literature [13,20–22].

Several recent studies investigated the effect of thickness on the photocatalytic efficiency by different methods. Chen et al. [8] prepared TiO_2 films by a sol-gel method and observed that increasing the film thickness within a certain range (up to 10 μm) could significantly improve the photocatalytic activity, in terms of 4-chlorobenzoic acid degradation for water purification. Krysa et al. [23] prepared transparent TiO_2 films by applying a dip-coating sol-gel process and found an increase in the photocatalytic-activity when increasing the thickness. Wu et al. [7] reported that photocatalytic activity is strongly correlated with the thickness of the coatings following the Langmuir-type kinetics in case of thin photocatalytic films, and the increased thickness promotes the photocatalytic efficiency. However, the effect on the degradation of air pollutants is not clear since the focus has been by far mainly paid to the water treatment.

The modification of TiO_2 with silica might be beneficial from several points, such as improved dispersibility, durability of the designed film and contribution to the enhanced photocatalytic properties [24,25]. The dispersibility relates mainly to the surface chemistry of the silica coating – paint/coating film interface and less to the characteristics of TiO_2 – silica interactions. The durability relates more to the photo-redox properties of TiO_2 and the consequent "damage" to organic resins in the paint/coating film [26]. The addition of silica can promote the durability of the coatings, especially if an organic binder is used [27]. Scalarone et al. [28] used tetraethoxysilane (TEOS), a silica precursor, as a coupling agent to improve the chemical stability of the dispersed TiO_2 nano-particles in water-based coatings and they observed a photocatalytic efficiency through discoloration of graffiti. Mo et al. [29] found the highest decomposition rate of toluene when TiO_2 was mixed with mordenite and SiO_2. In addition, they observed that the hybrid photocatalyst was porously distributed. The influence of silica modification on the photocatalytic activity of TiO_2 incorporated into a water based acrylic coating was also reported by [13,16]. The results revealed that silica modification effectively reduces the photocatalytic activity of the TiO_2 on the coatings' formulation and by doing so retards the coatings' degradation. Other researchers confirmed that the porous structure of the silica might enhance the photocatalytic activity [25,30,31]. However, the combined effect of the silica modification and the dosage of the photocatalytic coating on the photocatalytic degradation of common air pollutants under indoor air conditions have not yet been studied to the authors' knowledge.

The present work aims to study the effect of the nano-silica modification and the effect of the photocatalyst dosage on the air pollutants removal efficiency under indoor air conditions. This was evaluated by the degradation of an inorganic model air pollutant (nitric oxide) for the indoor application. The developed coatings were applied by the wire-wound coating method since it is one of the most popular techniques in use today, next to gravure and reverse roll coating, especially because of the precise thickness control ability of this technique [32]. A wallcovering was chosen as the carrier for the photocatalytic coating, because of its wide application in indoor environments and its direct contact with ambient air and light. A photocatalytic suspension containing 40% carbon-doped titanium dioxide (C–TiO_2) and a colloidal suspension containing 40% of nano-silica were applied. The starting materials and the developed applied coatings were characterized by particle size, elemental composition, morphology and light reflectance analyses. The effect of the silica modification and the amount of the applied coating were analyzed by photocatalytic efficiency assessment following a modified procedure based on ISO 22197-1 standard as a reference. The modification of the standard procedure was done in order to more closely represent a realistic indoor air condition. A pre-treatment method was applied on the coatings to promote the photocatalytic efficiency of the developed coatings. The pre-treatment was assessed prior to the photocatalytic assessment under visible light condition. The air pollutants removal efficiency and the reaction rate of the developed coatings were evaluated and discussed.

2. Experimental

2.1. Materials

A trial water-based suspension, KRONOClean 7404, containing visible-light responsive carbon-doped titanium dioxide (designated KC; provided by Kronos International) [33], was used as the photocatalyst. The KC consists of 40% of solids (mostly C–TiO_2), has a pH of 7–8 (at 20 °C), flash point >90 °C, a density of 1.35–1.55 $g \cdot cm^{-3}$ (at 20 °C) and dynamic viscosity <800 mPas. In addition, certain surfactants were applied in the suspension in order to keep the stability of the nano particles. A colloidal suspension of nano-silica was applied. The silica suspension is a water-based suspension of nano-silica containing 40% of solids. It has a pH of 9.2–9.9 and a density of 1.3 $g \cdot cm^{-3}$ (at 25 °C). The carrier, on which the coatings were applied, is wallcovering consisting of a paper substrate coated with a layer of polyvinylchloride (PVC; provided by BN International). The gas mixtures used for the experiments were prepared by mixing nitric oxide (50 ppm in nitrogen) with a synthetic air (Praxair) under the pressure of 1.0–1.2 bar.

2.2. Preparation of the coatings

Two series of coatings were prepared, applied and evaluated. The coatings made with the KC suspension without any modification were designated KC. The coatings containing the KC suspen-

sion modified with 10 mass% of silica (relative to C–TiO_2 mass) were designated KCS. Silica modification was achieved by high-energy mixing of the KC suspension for 20 min under 5000 rpm and drop wise addition of silica suspension in the first 60 s. The mixing was performed by using a high-energy mixer (L5M, Silverson) equipped with a square-hole high-sheer screen head suitable for the preparation of emulsions and fine colloidal suspensions.

The coatings were applied on top of the prepared carrier by a drawdown coating method, applying a wire-wound metering rod. A wallcovering carrier (WP) with dimensions of 200 × 100 mm^2 was used. A wire-wound metering rod type US4 was used for all coating applications. The US4 metering rod coats one layer with a wet thickness of 8 μm. The coating was applied manually by drawing it down with the wire-wound metering rod using an adequate and even force and speed. Each formulation was applied on the WP in one (L1), two (L2) or three (L3) layers in order to increase a dosage of the developed coating. The wet coating thicknesses and dosages based on the density of the applied materials and the wire-wound coating rod US4 is presented in Table 1. The corresponding amount of the applied photocatalyst and silica is discussed in Section 3.1. Every applied layer was cured prior to further actions. The curing was achieved by an infrared irradiation (IR) generated by an IR dryer TEXFLASH (Acos Graf) with a 6000 W infrared heat source. The measured temperature on the surface of the irradiated coatings, with a distance of 10 cm from the irradiation source, after 20 s under the full power of the IR dryer was about 150 °C.

The application and curing procedure are as follows: the carrier was pre-heated by IR for 10 s in order to increase the adhesion of the PVC to the developed coatings; then the coating was applied; and afterwards cured by IR for 20 s. In case of multiple layers application, the curing procedure was applied after each coated layer followed by the cooling down of the sample. Then the prepared samples were stored in the dark until further actions.

2.3. Characterization

The particle size distribution (PSD) was measured by applying the Dynamic Light Scattering (DLS) technique using a Zetasizer Nano ZS (Malvern). The samples were diluted with demineralized water to meet the criteria of the analytical instrument and they were measured in the 10 × 10 × 45 mm^3 polystyrol/polystyrene cuvettes.

In order to determine the composition of the materials and to confirm the amount of the TiO_2 and SiO_2 particles, an elemental analysis was performed, by an energy dispersive X-ray fluorescence (EDXRF) spectrometer/Epsilon 3 range (PANalytical). The Omniam program was used for the analysis. The samples were firstly dried in the oven under the temperature of 95 °C until the mass was constant, then milled and analyzed in a pressed powder form.

The morphology of the applied coatings was analyzed by a scanning electron microscope QUANTA FEG (FEI Company). This was followed by the elemental mapping analysis performed by an energy dispersive X-ray spectroscope (EDAX) operated by GENESIS software (EDAX). The analyses were performed on the cured KC and KCS samples applied on the wallcovering carrier. The samples were cut into the required size, analyzed and compared. The KC-L1 coating distribution was analyzed by 3D analysis applying a digital microscope VHX-700F series (Keyence).

In order to evaluate the composition effect of the coatings and the effect of the pre-treatment towards light, a diffusive reflection experiments were performed. A USB4000 spectrometer HL-2000 and a Tungsten Halogen light source (OceanOptics) optimized for the VIS-NIR (360–2500 nm) range were used. A reflection probe holder modified to hold probe in 45 degrees from the measured surface was applied. The reflectance range was fixed to 400–700 nm, as the developed photocatalytic coating is used for indoor air purification. The SpectraSuite® spectrometer operating software was used for the data collection. The WS-1 diffuse reflectance standard was used as a reference under light and dark conditions.

Table 1
Composition and calculated dosages of the tested coatings.

C–TiO_2 [%]	SiO_2 [%]	Designation	Wet coating thickness [μm]	Wet coating dosage [mg·cm^{-2}]
40	–	KC-L1	8	1.15
		KC-L2	16	2.30
		KC-L3	24	3.46
36.4	3.63	KCS-L1	8	1.16
		KCS-L2	16	2.32
		KCS-L3	24	3.48

2.4. Pre-treatment

A previous research [18] showed that the PCO efficiency could be greatly suppressed due to the coverage of the photocatalyst by, for instance, organic groups present in the coatings. Therefore, a pre-treatment procedure was implemented here to degrade the surfactant (organic groups), in order to expose the photocatalytic particles to environment to promote the photocatalytic efficiency of the coatings. The pre-treatment was carried out by irradiating the samples by the ultraviolet (UV) light for a certain period in order to degrade the hindering layer and to expose the photocatalytic particles. The applied light source was composed of three fluorescent tubes of 25 W each, emitting UV-A radiation (300–400 nm), set to the light intensity of 10 W·m^{-2} measured in UV-A region close to the surface of the tested samples.

In order to assess the efficiency of the UV pre-treatment and to establish an optimal pre-treatment duration, samples were embedded in a plug-flow reactor, as presented in Fig. 1. During the UV irradiation, a model pollutant – 1 ppm of nitric oxide – was introduced under the flow of 1.5 L·min^{-1} and the reduction of the concentration (photocatalytic efficiency) in time was monitored. The reduction of the model pollutant concentration relative to the UV irradiation duration, coating composition (with or without silica) or the amount of the applied coating was analyzed. The photocatalytic efficiencies after various times of UV irradiation were analyzed in order to determine the optimal pre-treatment duration. The measurements were performed in duplicate and average results were presented.

2.5. Photocatalytic assessment

The photocatalytic oxidation (PCO) efficiency was assessed by the NO removal experiments using a plug-flow experimental setup [9] in accordance with the ISO 22197-1 standard. Since the experimental conditions specified in ISO standard are far from the real indoor conditions, some of them (inlet pollutant concentration, flow rate, light source) were modified in order to closely simulate the indoor environment. Nitric oxide (NO) was used as a model pollutant and it was mixed with a synthetic air to an inlet concentration of 100 or 500 ppb under the flow rate of 1–3 L·min^{-1}. The applied light source was composed of three fluorescent cool daylight lamps (VIS) of 25 W each, emitting a visible light irradiation with the wavelength 400–700 nm, set to the intensity of 10 W·m^{-2} measured in a blue-green light region close to the surface of the testing samples. The experimental conditions, such as the pollutant concentration, flow rate, humidity and light intensity were fully controlled. The temperature and the relative humidity were measured at the inlet of the reactor. The outlet concentration of model pollutant NO and the possible production of an interme-

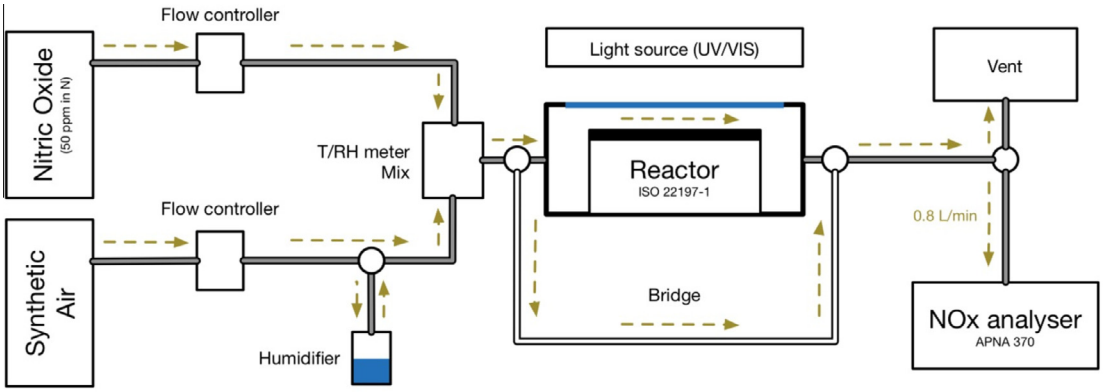

Fig. 1. Plug-flow experimental set-up scheme.

diate NO_2 were measured and interpreted as NO_x concentration. The measurements were performed in duplicate and the average results were presented. Fig. 1 shows the scheme of the plug-flow experimental set-up.

The concentration of pollutants (NO and NO_2) was measured by an online NO_x analyzer APNA-370 (Horiba). The APNA-370 continuously monitors the NO_x concentration using a cross-flow modulated semi-decompression chemiluminescence method. The concentration measurement was performed automatically every 5 s with a sampling rate of 0.8 $L{\cdot}min^{-1}$. The development of the NO_x concentration during the experiment was presented and the final degradation efficiency was calculated and compared. The reaction mechanism of PCO of NO_x has been presented elsewhere [34]. Thanks to the high light reflectance of the applied nano-silica, the photocatalytic efficiency can be potentially enhanced as it increases the production of the electron/hole pairs, and this is investigated in the present study.

2.6. Photocatalytic efficiency assessment

In the present study, the photocatalytic efficiency was evaluated following different approaches. The direct NO_x degradation was calculated following the current standard (ISO 22197-1) to provide a direct information on the air pollutants removal efficiency, furthermore the reaction rate and reaction order were analyzed to understand the intrinsic performance of the developed air purifying coating.

2.6.1. Determination of direct degradation (%)

The photocatalytic efficiency of the tested samples was evaluated by the amount of NO_x ($NO + NO_2$) removed (difference between the initial and final concentration), calculated using the following equation:

$$NO_x\,\text{degr.} = \eta_{NO_x} \times 100[\%] \tag{1}$$

where η_{NO_x} is the conversion of the NO_x in the steady state calculated as:

$$\eta_{NO_x} = 1 - \frac{C_{(NO_x)_{out}}}{C_{(NO_x)_{in}}} \tag{2}$$

where the initial NO_X concentration $(C_{NO_x})_{in}$ was taken as an average value of 5 min before turning on the light. The outlet NO_X concentration $(C_{NO_x})_{out}$ was taken as an average value of the last 5 min of the irradiation period.

In order to compare the results, NO degradation efficiency was also evaluated here using the following equation:

$$\text{NO degr.} = \eta_{NO} \times 100[\%] \tag{3}$$

where η_{NO} is the conversion of the NO in the steady state computed as:

$$\eta_{NO} = 1 - \frac{C_{(NO)_{out}}}{C_{(NO)_{in}}} \tag{4}$$

where the initial NO concentration $(C_{NO})_{in}$ was taken as an average value of 5 min before turning on the light. The outlet NO concentration $(C_{NO})_{out}$ was taken as an average value of the last 5 min of the irradiation period.

2.6.2. Determination of reaction order

The main limitation for laminar flow conditions is the transport of the gas-phase reactant to the photocatalytic surface, leading to the formation of concentration gradients for fast heterogeneous reactions [35]. The gas phase diffusion limitation can be corrected if the reactive uptake (for definition see Eq. (17)) is not too high (for ISO reactor $\gamma > 10^{-5}$) [36].

The reaction order was determined following the method used by Ifang et al. [36], where a logarithm of the concentration was plotted against t_{rxn}. In that study, slow first-order loss of O_3 was observed, for which the logarithm of the concentration was linearly correlated with t_{rxn}. The reaction order in the current study was determined on KCL3 and KCSL3. The reaction time (t_{rxn}) was varied from 2.4 to 1.2 s, corresponding to 1.5 to 3 $L{\cdot}m^{-1}$, respectively. The NO concentration was set to 0.5 and 0.1 ppm in order to evaluate the initial pollutant concentration effect. The aim was to reach a linear correlation, which would represent the first order kinetics.

2.6.3. Determination of reaction rate ($mg{\cdot}h^{-1}{\cdot}m^{-2}$)

In order to evaluate the reaction rate, a series of NO_x degradation experiments under the fixed NO concentration and various flow rates were performed following the method troduced by Minero et al. [37]. Based on the assumption that the reaction is of first order, the reaction rate $r_{(C_o)}$ was calculated using the following equation [37]:

$$r_{(C_o)} = \frac{C_{(NO)_{in}} \cdot F}{S_{active}} \ln\left(\frac{1}{1-\eta_{NO}}\right)\left[\text{mg}\cdot\text{h}^{-1}\cdot\text{m}^{-2}\right] \tag{5}$$

where $C_{(NO)_{in}}$ is the initial NO concentration [$mg{\cdot}m^{-3}$], F is the flow rate [$m^3{\cdot}h^{-1}$] and S_{active} is the active area of the sample [m^2].

2.6.4. Reactive uptake coefficient evaluation

The reactive uptake coefficient is defined as the ratio of number of collisions that lead to reaction over all collisions of the gas-phase reactant with a reactive surface and it is calculated by the following equation [36]:

$$\gamma = \frac{4 \cdot k_{rxn}}{\bar{v} \cdot S_{active}/V} \quad (6)$$

where V is the volume of the reactor [m^3], $\bar{v}$ is the mean molecular velocity of the reactant [$m \cdot s^{-1}$] and k_{rxn} is the first-order rate coefficient [s^{-1}]. $\bar{v}$ and k_{rxn} were calculated based on Eqs. (19) and (20), respectively.

$$\bar{v} = \sqrt{\frac{8 \cdot R \cdot T}{\pi \cdot M}} [m \cdot s^{-1}] \quad (7)$$

where R is the ideal gas constant ($R = 8.314\ J \cdot mol^{-1} \cdot K^{-1}$), T is the absolute temperature [K] and M is the molecular mass of the reactant [$kg \cdot mol^{-1}$].

$$k_{rxn} = -\frac{\ln\left(\frac{c_{(NO)_{out}}}{c_{(NO)_{in}}}\right)}{t_{rxn}} \quad (8)$$

where t_{rxn} is the reaction time of the gas-phase reactant and the sample [s].

3. Results

3.1. Characterization

The particle size distribution of the KC suspension is uni-modal with the average particle size of 61 nm and a polydispersity index of 0.194. The particle size distribution of KCS formulation was measured, being also uni-modal, with the average particle size of 63 nm and polydispersity index of 0.197. These results indicated that the silica particles were attached to the C–TiO_2 particles, because the particle size analysis of the pure silica suspension revealed that the silica particles were 20 nm average in size. This is in line with Furlong et al. [26] who stated that TiO_2 dispersed in aqueous solution can be effectively coated by silica merely by allowing an aqueous dispersion of TiO_2 to equilibrate in a Pyrex vessel.

The results of the elemental analysis of the coatings in a dry state showed that KC consists of 98.13% of TiO_2 and 0.26% of SiO_2, while the trace amount of SiO2 is resulted from the preparation of the nano-suspension by colloidal milling method. KCS consists of 87.66% of TiO_2 and 10.34% of SiO_2. The residual compounds were characterized as ZrO_2 (0.56–0.64%), Ag_2O (0.20–0.21%), Al_2O_3 (0.03–0.12%) and CaO (0.16–0.17%). The SiO_2 content was clearly enhanced in case of KCS formulation. Table 2 summarizes the calculated dosages of TiO_2 and SiO_2 related to the type of formulation and the amount of the applied coating. The dosage of C–TiO_2 ranges from 0.407 to 1.356 $mg \cdot cm^{-2}$ and that of SiO_2 ranges from 0.001 to 0.144 $mg \cdot cm^{-2}$.

Fig. 2 shows the images of the applied coatings on the wallcovering. It is clear that increasing the dosage of the coating leads to a loss of the transparency of the coating due to the contained high amount of solids. Moreover, the coatings distribution on the carrier is not even, which suggests the need of wetting agents in order to improve the wetting ability and reduce the high surface tension of the suspensions.

The visual analysis (Fig. 3) revealed an uneven distribution of the coating (darker regions in the images) in case of coatings coated in lower dosages. The distribution was clearly improved when the coating dosage increased, especially in case of coatings containing silica (KCS-L3), which can be attributed to the improved thermal stability [38]. A certain amount of micro cracks was observed in all coatings. Nevertheless, the increased amount of cracks can improve the photocatalytic efficiency by increasing the surface of the coating exposed to the environment. A modified composition with a reduced viscosity leading to improved distribution with a thinner coating layer [14], or a modified curing method will be tested in the future study.

Fig. 4 shows the results of the surface analysis of the applied coatings. The analysis confirms that the coatings are not evenly distributed, which could be caused by the high viscosity of the suspensions or by the curing method as a result of contraction, stress and different thermal expansion coefficients of the top-layer and the carrier as was also observed elsewhere [14,39]. This led to the formation of un-coated parts, in case of coatings coated in lower dosages (KC-L1 and KCS-L1). The formation of cracks led to an increased roughness of the coatings, especially in the case of coatings containing silica applied in higher dosage (KCS-L3), which can be seen in Fig. 4d. This increases the exposed surface of the coating and it can improve the light distribution within the coating, which improves the photocatalytic efficiency. In addition, the profile analysis of the coatings shows that the roughness increases with the increasing dosage of the coating, which results in more active surface.

The scanning electron microscope (SEM) and the results of the Ti elemental mapping images of the KC-L1, KC-L3, KCS-L1 and KCS-L3 focusing on Ti are presented in Fig. 5. The elemental mapping analysis of the KC and KCS coatings confirms the uniform dispersion of Ti, in case of KC, and uniform dispersion of Ti and Si, in case of KCS coatings, within the matrix of the coatings. This is mainly because the TiO_2 and SiO_2 were incorporated in the form of stabilized nano-suspension. The uncoated spots in case of KC-L1 and KCS-L1 (indicated by white regions) confirm the uneven distribution of the coatings observed during the SEM analysis. This was not observed when the coatings were applied in higher dosages (KC-L3 and KCS-L3).

Fig. 6 shows the results of the light reflectance measurements performed on the wallcovering carrier (WP) and wallcovering carrier coated with KC and KCS coatings before (NT) and after 10 h UV pre-treatment (UV) in the 400–700 nm light wavelength range. The results show that the amount of the applied coating has an effect on the reflectance, which is caused by the increased roughness of the coating, observed in the previous section (Fig. 4). The nano-silica modification led to an increased reflection as well. The increased reflection can lead to an improved light distribution within the coating, resulting in a better photocatalytic activation of the coatings. The UV pre-treatment led to a higher reflection in coatings coated in a higher dosage (KC-L3 and KCS-L3). This suggests that the pre-treatment exposed the incorporated nano-silica and TiO_2 by degrading the surfactant surrounding it, which results in an increased roughness of the surface leading to even increased reflection.

Table 2
C–TiO_2 and SiO_2 dosages of the developed coatings.

Designation	Dosage [$mg \cdot cm^{-2}$]	
	C–TiO_2	SiO_2
KC-L1	0.452	0.001
KC-L2	0.905	0.002
KC-L3	1.356	0.004
KCS-L1	0.407	0.048
KCS-L2	0.813	0.096
KCS-L3	1.221	0.144

3.2. Pre-treatment assessment

Fig. 7 shows the UV pre-treatment efficiency results of the KC-L1-3 and KCS-L1-3 coatings after 2, 5, 7 and 10 h of UV irradiation ($10\ W \cdot m^{-2}$). The results clearly show that the UV pre-treatment promotes the photocatalytic efficiency. The UV irradiation degrades the surfactant layer, which covers the photocatalytic par-

Fig. 2. Images of the carrier (WP) and the applied coatings (KC-L3 and KCS-L3).

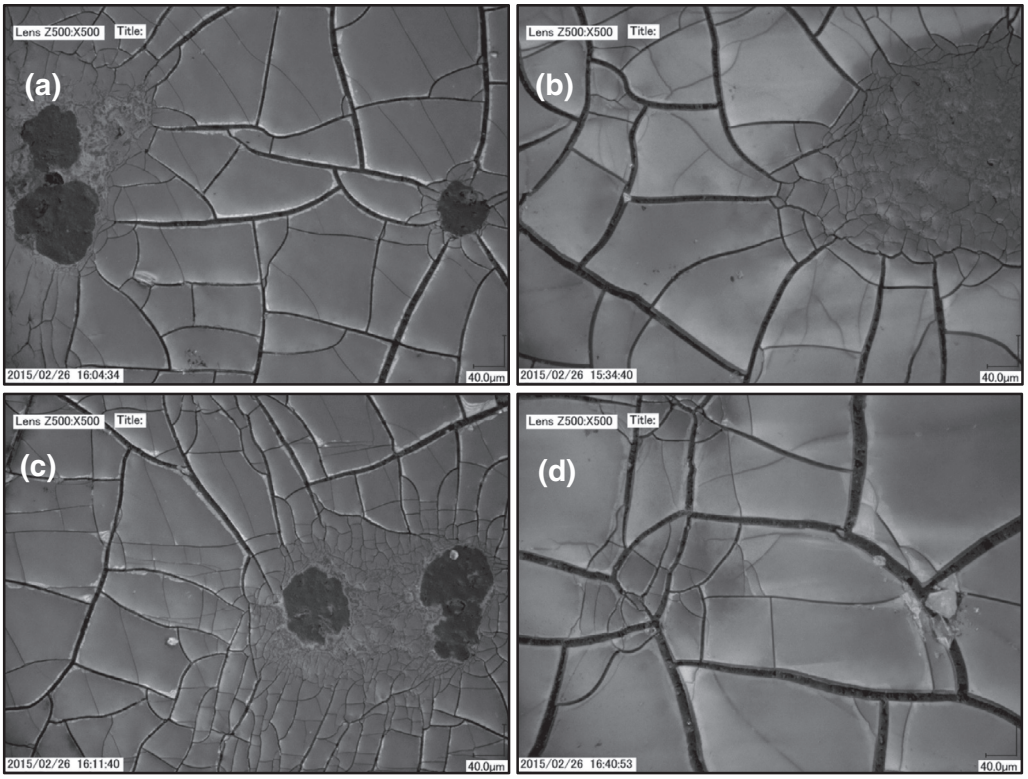

Fig. 3. Images of the applied coatings: a) KC-L1; b) KC-L3; c) KCS-L1; d) KCS-L3.

ticles, and exposes them to the environment. The efficiency of the pre-treatment is dependent on the duration of the irradiation, the amount of the applied coating and the silica content.

The samples coated with only one layer showed their peak PCO performance after about 7 hours' UV irradiation, degrading around 60% (KC-L1) and 30% (KCS-L1) of NO_x. Their efficiency dropped afterwards due to the deactivation caused by the high concentration of the applied model pollutant, which resulted in deactivation of the photocatalyst. This is in line with the work of Ohko et al. [40], who concluded that the deactivation caused by the accumulation of HNO_3 was proportional to the thickness of the photocatalytic coating. The most efficient coatings after the 10 hours' UV pre-treatment were the coatings applied in two layers, which suggests that the UV pre-treatment efficiency is dependent on the dosage of the coating. The NO_x removal efficiency was after 2 h of irradiation about 1% (KC-L2) and 3% (KCS-L2), however, the efficiency rapidly increased in time resulting in high NO_x removal efficiency of 74% (KC-L2) and 67% (KCS-L2) after 10 h of irradiation. The samples made with three layers showed high NO_x degradation efficiency of 46% (KC-L3) and 62% (KCS-L3). The results indicate that samples coated in two and three layers require a longer pre-treatment in order to reach their maximum potential, which can be seen by the increased tendency of PCO efficiency in time of the UV pre-treatment termination. The coatings made with three layers (KCS-L3) had significantly better PCO efficiencies than the unmodified one (KC-L3), which can be attributed to the better coating distribution, as was discussed in the Section 3.1. After 10 h of irradiation, the differences in NO_x degradation between KC and KCS coatings were +25%;+7%; and −16% for L1; L2; and L3, respectively.

The PCO activation rate is shown in Fig. 7b. It can be obviously seen the effect of the photocatalysts layer and the dosage of nano-silica. Increasing the coating dosage caused a delay in the PCO activation rate, which can be well observed e.g. on the KC-L1 and KC-L3 in the Table 3, where the activation started at 2.5 and 5.1 h after

Table 3
PCO activation times of KC/KCS-L1-3.

Applied layers	Activation time [h]	
	KC	KCS
L1	2.5	2.1
L2	2.9	2.6
L3	5.1	3.7

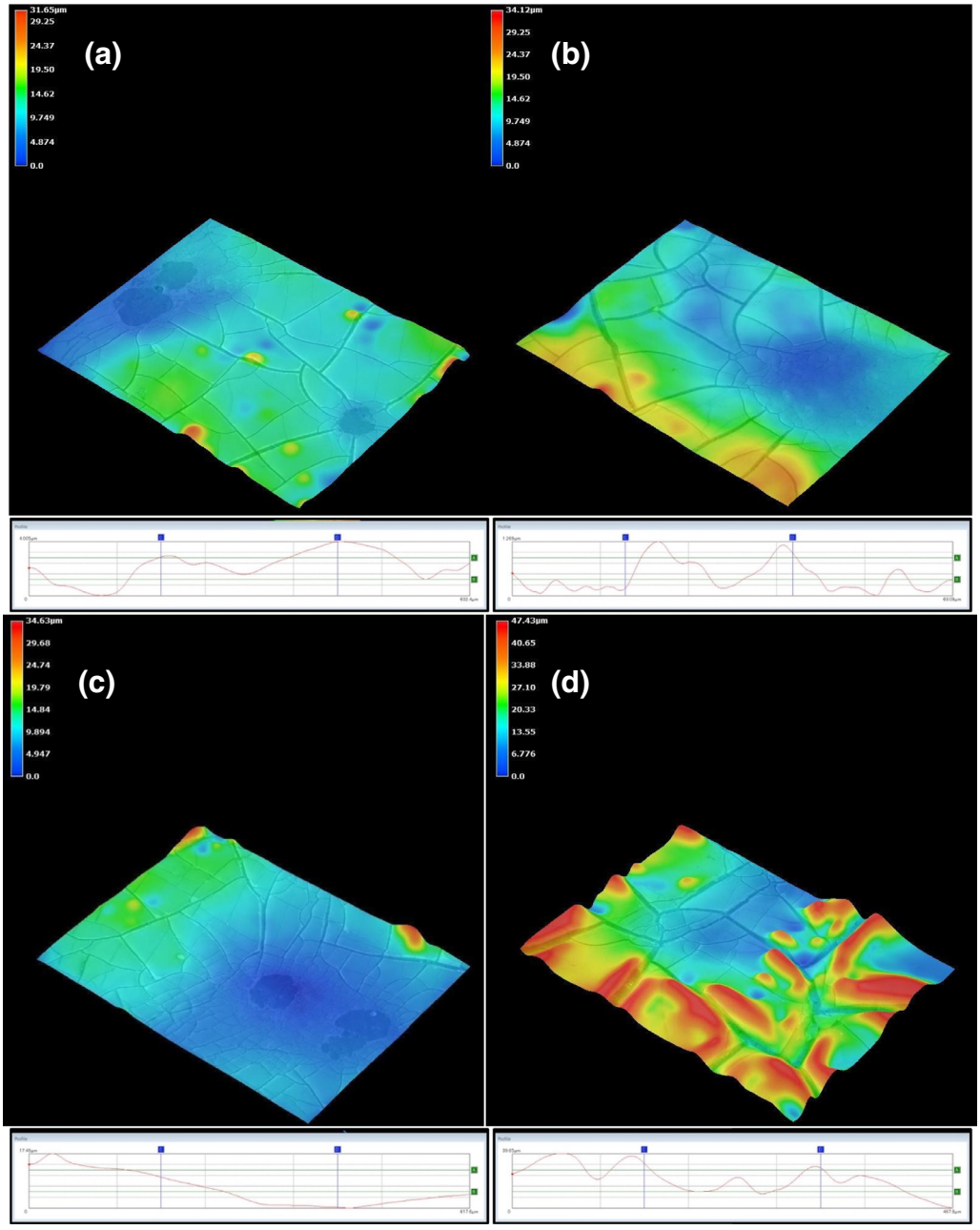

Fig. 4. Images of the surface analysis: a) KC-L1; b) KC-L3; c) KCS-L1; d) KCS-L3.

the start of the irradiation, respectively. This can be explained by the increased amount of the surfactant above the C–TiO_2 particles. The silica modification shortened the activation time, e.g. to 2.1 and 3.7 h for KCS-L1 and KCS-L3, respectively. The shortened activation time can be explained by the improved distribution of the coating (as was seen in the Fig. 6), resulting in a thinner layer of the coating, or by the improved UV light scattering caused by the presence of silica particles.

3.3. Photocatalytic assessment

3.3.1. NOx degradation rate according to ISO 22197-1

The results of the NO removal tests on the KC/KCS-L1-3 pre-treated samples, tested under the visible light irradiation (10 $W \cdot m^{-2}$), the flow rate of 1.5 $L \cdot min^{-1}$ and the initial NO concentration of 0.1 and 0.5 ppm are presented in the Figs. 8 and 9. The results are presented as NO/NO_X degradation efficiency (%) dependent on the amount of applied layers.

The results show that the pre-treated KC coatings exhibited very good NO degradation efficiencies of 24–47% under 0.5 ppm and 36–62% under 0.1 ppm. The KCS coatings show higher NO degradation efficiencies of 34–65% under 0.5 ppm and 47–78% under 0.1 ppm. The NO_X degradation results show that the coatings still possess high degradation efficiencies of 15–30% under 0.5 ppm and 23–44% under 0.1 ppm for KC and 21–48% under 0.5 ppm and 32–61% under 0.1 ppm for KCS coatings.

The highest NO degradation is reached by the two-layered coatings (KC/KCS-L2). The higher efficiency in case of two-layered coatings is in line with UV pre-treatment results. The silica modification promoted the PCO efficiency, as the maximal NO removal was measured as 62% for KC-L2 and 78% for KCS-L2 under initial NO concentration of 0.1 ppm. This was observed elsewhere

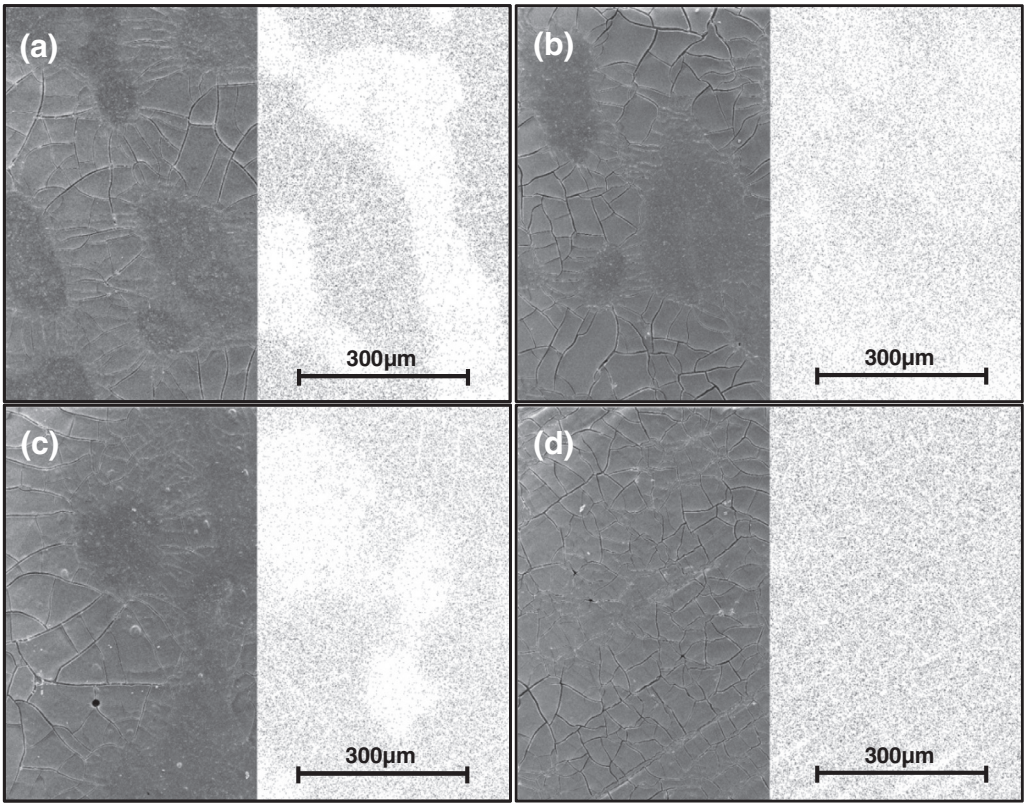

Fig. 5. SEM analysis of: a) KC-L1; b) KC-L3; c) KCS-L1; d) KCS-L3.

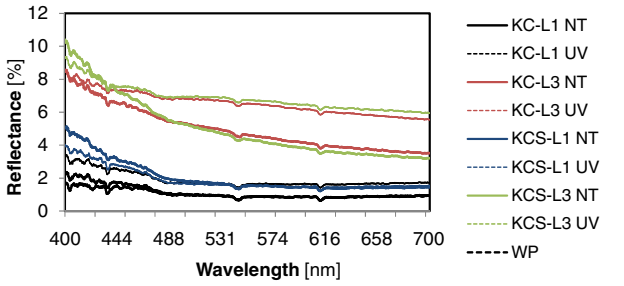

Fig. 6. Reflectance measurement results before (NT) and after UV pre-treatment (UV).

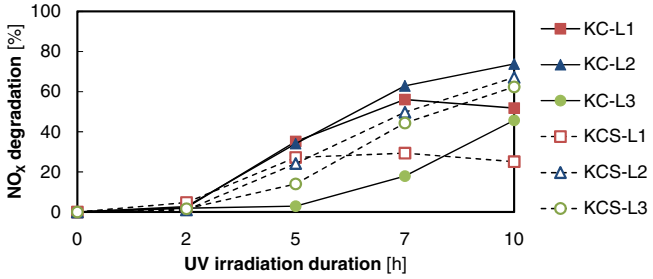

Fig. 7a. NO_x degradation results of KC-L1-3 and KCS-L1-3 tested under UV irradiation.

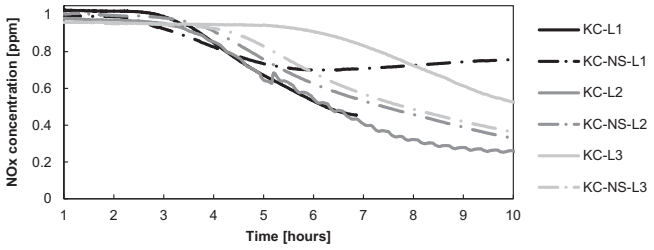

Fig. 7b. Photocatalytic activation results of the developed coatings.

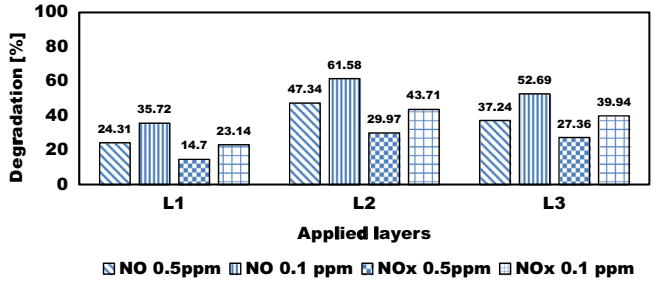

Fig. 8. KC-L1-3 NO/NOX degradation efficiencies under VIS and 0.5/0.1 ppm of NO.

as well [41]. The improved photocatalytic efficiency can be attributed to the improved light distribution, improved pollutant absorption [22], better distribution of the coating due to the increased layer number [38], or the high surface area of the nano-silica, which can potentially enhance catalytic activity by making more TiO_2 surface readily available to reactants [42]. The increased coating dosage had a profound effect on the PCO efficiency, which was also reported by other researchers [7,8,43].

3.3.2. Reaction order determination

The results of the reaction order determination are presented in Fig. 10. The results show that the chosen reactor and experimental conditions lead to a linear dependence with an intercept in zero

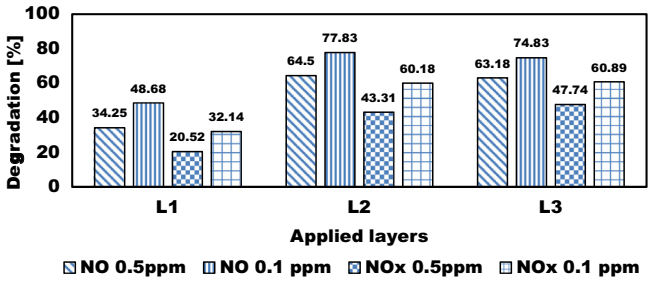

Fig. 9. KCS-L1-3 NO/NOX degradation efficiencies under VIS and 0.5/0.1 ppm of NO.

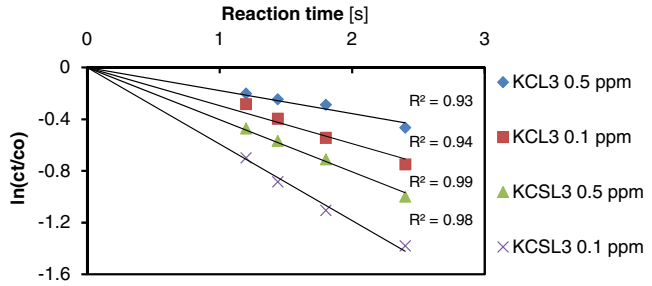

Fig. 10. Degradation of NO under various conditions (0.5/0.1 ppm of NO; flow rate of 1.5–3 L/min).

with a very good fit (above $R^2 = 0.93$). It is concluded that reactions on the developed coatings follow the first-order kinetics in the applied plug-flow reactor [36]. The results also show that the different initial pollutant concentration leads to different slope of the curve.

3.3.3. Reaction rate determination

Based on the results above, it can be concluded that the NO degradation follows the first order and therefore Eq. (3) is used for the calculation of the normalized rate $r_{(Co)}$. The calculated normalized rates were independent of the flow rate (see Appendix A). The calculated average values are listed in Table 4.

These values clearly show that KCSL3 is indeed more efficient in NO degradation than the KCL3 sample. The values presented in this section are comparable with any material tested under any plug-flow conditions, taking in mind that experiments should following the first order kinetics.

3.3.4. Reactive uptake coefficient

In order to compare the results of different samples tested under different conditions and different reactors, a dimensionless reactive uptake coefficient (γ) was calculated for KC/KCSL3 following Eq. (5). The results of the γ values were independent of the flow rate (see appendix). The calculated average values are listed in Table 5.

The results confirmed that the KCSL3 coatings are more efficient in degradation of NO than the KCL3. The values presented in this section are comparable with any material tested under any conditions, taking in mind that the compared experiment is following the first order kinetics.

Table 4
Normalized rate values [$mg \cdot h^{-1} \cdot m^{-2}$] for KC/KCS-L3 under 0.5/0.1 ppm of NO.

Sample	0.5 ppm		0.1 ppm	
	Average	Standard deviation	Average	Standard deviation
KCL3	1.21	0.10	0.39	0.05
KCSL3	2.78	0.08	0.83	0.03

Table 5
Normalized rate values for KC/KCS-L3 under 0.5/0.1 ppm of NO.

Sample	0.5 ppm		0.1 ppm	
	Average	Standard deviation	Average	Standard deviation
KCL3	4.5E−06	3.8E−07	7.4E−06	8.8E−07
KCSL3	1.0E−05	3.0E−07	1.6E−05	5.4E−07

4. Discussion

The C–TiO_2 suspension (KC) or the silica-modified KC (KCS) was applied on the wallcovering carrier in various dosages. The characterization of the primary materials and the silica modification revealed nano-scale particle distribution in both KC and KCS, which is beneficial for the visual appearance of both, creating transparent layers and beneficial for the photocatalyst distribution leading to a higher photocatalytic efficiency, because of the enhanced amount of active sites [9]. The elemental mapping analysis confirmed the uniform distribution of photocatalyst and the presence of silica particles, which is beneficial in terms of durability [26].

The UV-pretreatment was found to be an efficient method in order to promote the PCO efficiency of the developed coatings. The results of the pre-treatment showed that the optimal pre-treatment duration is dependent on the amount of the applied coating and on the silica modification. The best performing coatings, which showed the maximal efficiency after the 10 h of pre-treatment, were the ones coated with two layers in both formulations. This suggests that the pre-treatment duration needs to be tailored to the dosage of the applied coating. The silica modification significantly shortened the PCO activation time, especially with the increasing dosage of the coating where the activation time was greatly decreased from 5 h (KC-L3) to about 3 h (KCS-L3). This can be attributed to the increased reflection of the light within the coating due to the silica content observed during the reflection measurements. The increased reflection can serve very well in indoor conditions where the light intensity from common light source is not as high as during the measurements. However, due to the high energy requirement during the UV pre-treatment, manners of pre-treatment will be considered as well in future study along with the incorporation of the currently tested designs into water-based acrylic coating. This can improve the workability and can lead to better final properties of the coatings.

The NO_x removal efficiency of the samples tested under indoor air conditions showed very high NO_x removal efficiencies. The silica modification had a good enhancement effect on the PCO efficiency with the NO degradation up to 65% (48% de-NO_x) under reduced conditions comparing to the ISO standard and up to 78% (61% de-NO_x) under realistic environmental conditions. These results are around 17% higher than the un-modified KC coatings, which degraded up to 47% and 62% of NO (30% and 44% de-NO_x) under similar conditions. These results are in line with other studies that showed beneficial effect of silica modification [18,20–22,44,45], where the focus was mainly paid to water treatment or self-cleaning effect. For instance, 40% methylene blue degradation increase [44], 62% organic dye degradation increase [45], or 37.5% more effective self-cleaning effect in case of silica-modified TiO_2 compared to the pure TiO_2 were observed. This beneficial effect is attributed to the better absorption [22]; better dispersion of the photocatalytic particles, resulting in the higher number of the active sites; and/or better utilization of the light, due to the macro/meso-porous structure of the coating. On the other hand, some studies show a significant decrease in the reaction rate [13,39], which can be in turn explained by the reduced active surface of TiO_2 by SiO_2 particles.

The representation of the PCO efficiency results according to the ISO standard is rather limited because only samples tested under completely same conditions can be compared. More scientifically based representation of the results is clearly necessary. Following the work from others [36,37], a reaction rate and reactive uptake coefficient are calculated here, to directly compare the results with samples tested under different conditions and even in different reactors. Based on the applied calculations, the developed coatings followed the first order kinetics under the applied conditions. The results of the reactive uptake coefficient compared to other results are considered relatively high since, e.g. [36] tested photocatalytic paint and mortar for NO degradation and reported reactive uptake coefficients of 4×10^{-5} and 1.4×10^{-5}, respectively. The results of different pollutant concentration are, however, not in line with the statement that the reactive uptake coefficient is independent of pollutant concentration [36]. The results clearly show that with increasing the pollutant concentration, the reaction rate is rising from 0.39 to 1.21 for KCL3 and 0.83 to 2.78 for KCSL3 and the reactive uptake coefficient is decreasing from 7.4E−06 to 4.5E−06 for KCL3 and 1.6E−05 to 1.0E−05 for KCSL3.

5. Conclusion

This article addresses the effect of the silica modification and photocatalytic coating dosage on the photocatalytic efficiency, for the application in indoor environment. In addition, a pretreatment method, in order to promote the photocatalytic efficiency, was applied and its efficiency was evaluated. The following conclusions can be drawn:

- The UV-pretreatment was found to be an effective PCO activation method for the developed coatings and it was found to be dependent on the amount of the applied coating and on the composition (silica content);
- The silica modification shortened the PCO activation time about 0.4, 0.3 and 1.4 h for 1, 2 and 3 layered coatings, respectively;
- The silica modification enhanced the PCO efficiency of about 17% in case of the best performing coatings;
- The best performing coatings (KCS-L2) degraded 65% and 78% of NO under the initial NO concentration of 0.5 and 0.1 ppm, respectively;
- The reaction rate and reactive uptake coefficient were calculated to interpret the photocatalytic efficiency of the developed coatings;
- The reaction rate was calculated for realistic conditions (0.1 ppm of NO) as 0.39 $mg \cdot h^{-1} \cdot m^{-2}$ and 0.83 $mg \cdot h^{-1} \cdot m^{-2}$ for KCL3 and KCSL3, respectively;
- The reactive uptake coefficient (γ) was computed as 7.4E−06 and 1.6E−05 under 0.1 ppm of NO for KCL3 and KCSL3, respectively.

Acknowledgements

This research was carried out under the project number M81.7.10405 in the framework of the Research Program of the Materials innovation institute M2i. The authors would like to acknowledge Wouter Post (PhD researcher at Delft University of Technology) for assistance with the 3D surface characterization. Moreover, the authors wish to express their gratitude to the following sponsors of the Building Materials research group at TU Eindhoven: Rijkswaterstaat Grote Projecten en Onderhoud; Graniet-Import Benelux; Kijlstra Betonmortel; Struyk Verwo; Attero; Enci; Rijkswaterstaat Zee en Delta-District Noord; Van Gansewinkel Minerals; BTE; V.d. Bosch Beton; Selor; GMB; Icopal; BN International; Eltomation; Knauf Gips; Hess AAC Systems; Kronos; Joma; CRH Europe Sustainable Concrete Centre; Cement & Beton Centrum; Heros; Inashco; Keim and Sirius International (in chronological order of joining).

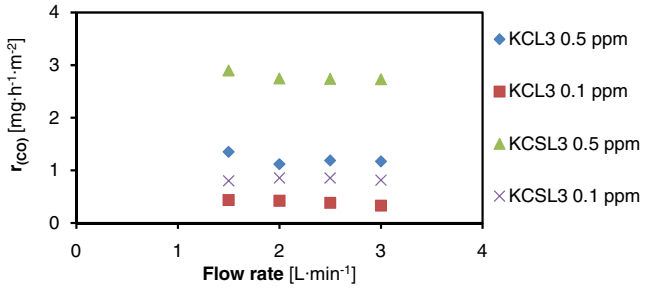

Fig. 11. Reaction rate versus flow rate.

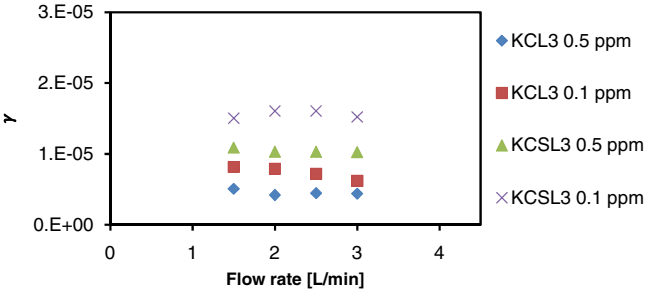

Fig. 12. Reactive update coefficient versus flow rate.

Appendix A.

Figs. 11 and 12.

References

[1] M. Sleiman, J.-M. Chovelon, P. Conchon, C. Ferronato, Photocatalytic oxidation of toluene at indoor air levels (ppbv): towards a better assessment of conversion, reaction intermediates and mineralization, Appl. Catal. B Environ. 86 (2009) 159–165.
[2] O. Debono, F. Thevenet, P. Gravejat, V. Hequet, C. Raillard, L. Lecoq, N. Locoge, Toluene photocatalytic oxidation at ppbv levels: kinetic investigation and carbon balance determination, Appl. Catal. B Environ. 106 (2011) 600–608.
[3] Q.L. Yu, H.J.H. Brouwers, Indoor air purification using heterogeneous photocatalytic oxidation. Part I: experimental study, Appl. Catal. B Environ. 92 (2009) 454–461.
[4] R. Dillert, J. Stötzner, A. Engel, D.W. Bahnemann, InfluDillert, R., Stötzner, J., Engel, A., & Bahnemann, D. W. (2012). Influence of inlet concentration and light intensity on the photocatalytic oxidation of nitrogen(II) oxide at the surface of Aeroxide® TiO2 P25. Journal of Hazardous Materials, 211–212, J. Hazard. Mater. 211–212 (Apr. 2012) 240–246.
[5] X. Zhao, L. Lv, B. Pan, W. Zhang, S. Zhang, Q. Zhang, Polymer-supported nanocomposites for environmental application : A review, Chem. Eng. J. 170 (2011) 381–394.
[6] A. Mills, G. Hill, M. Crow, S. Hodgen, Thick titania films for semiconductor photocatalysis, J. Appl. Electrochem. 35 (7–8) (Jul. 2005) 641–653.
[7] C.-Y. Wu, Y.-L. Lee, Y.-S. Lo, C.-J. Lin, C.-H. Wu, Thickness-dependent photocatalytic performance of nanocrystalline TiO2 thin films prepared by sol–gel spin coating, Appl. Surf. Sci. 280 (Sep. 2013) 737–744.
[8] Y. Chen, D.D. Dionysiou, Correlation of structural properties and film thickness to photocatalytic activity of thick TiO2 films coated on stainless steel, Appl. Catal. B Environ. 69 (1–2) (Dec. 2006) 24–33.
[9] G. Hüsken, M. Hunger, H.J.H. Brouwers, Experimental study of photocatalytic concrete products for air purification, Build. Environ. 44 (12) (2009) 2463–2474.
[10] N.S. Allen, M. Edge, J. Verran, J. Stratton, J. Maltby, C. Bygott, Photocatalytic titania based surfaces: environmental benefits, Polym. Degrad. Stab. 93 (9) (Sep. 2008) 1632–1646.
[11] Y. Paz, Application of TiO2 photocatalysis for air treatment: patents' overview, Appl. Catal. B Environ. 99 (3–4) (Sep. 2010) 448–460.

[12] A. Goldschmidt, H.-J. Streitbeger, BASF Handbook on Basics of Coating Technology (American Coatings Literature). Vincentz, 2003.
[13] A. Mirabedini, S.M. Mirabedini, A.A. Babalou, S. Pazokifard, Synthesis, characterization and enhanced photocatalytic activity of TiO2/SiO2 nanocomposite in an aqueous solution and acrylic-based coatings, Prog. Org. Coat. 72 (3) (Nov. 2011) 453–460.
[14] J. Bennani, R. Dillert, T.M. Gesing, D. Bahnemann, Physical properties, stability, and photocatalytic activity of transparent TiO2/SiO2 films, Sep. Purif. Technol. 67 (2009) 173–179.
[15] M. Sökmen, I. Tatlıdil, C. Breen, F. Clegg, C.K. Buruk, T. Sivlim, S. Akkan, A new nano-TiO2 immobilized biodegradable polymer with self-cleaning properties, J. Hazard. Mater. 187 (1–3) (Mar. 2011) 199–205.
[16] S. Pazokifard, M. Esfandeh, S.M. Mirabedini, M. Mohseni, Z. Ranjbar, Investigating the role of surface treated titanium dioxide nanoparticles on self-cleaning behavior of an acrylic facade coating, J. Coat. Technol. Res. 10 (2) (Jul. 2012) 175–187.
[17] M. Sabzi, S.M. Mirabedini, J. Zohuriaan-Mehr, M. Atai, Surface modification of TiO2 nano-particles with silane coupling agent and investigation of its effect on the properties of polyurethane composite coating, Prog. Org. Coat. 65 (2) (Jun. 2009) 222–228.
[18] D. Gregori, I. Benchenaa, D. Leonard, S. Therias, J.-L. Gardette, C. Brunon, S. Parola, C. Guillard, Photocatalytic textiles for water and air depollution, 8th European Meeting on Solar Chemistry and Photocatalysis - Environmental Applications, 2014, pp. 95–96.
[19] S. Lorencik, Q.L. Yu, H.J.H. Brouwers, Design and performance evaluation of the functional coating for air purification under indoor conditions, Appl. Catal. B Environ. 168–169 (Jun. 2015) 77–86.
[20] M. Bellardita, M. Addamo, A. Di Paola, G. Marcì, L. Palmisano, L. Cassar, M. Borsa, Photocatalytic activity of TiO2/SiO2 systems, J. Hazard. Mater. 174 (1-3) (Feb. 2010) 707–713.
[21] L. Pinho, M.J. Mosquera, Photocatalytic activity of TiO2–SiO2 nanocomposites applied to buildings: influence of particle size and loading, Appl. Catal. B Environ. 134–135 (May 2013) 205–221.
[22] L. Zhou, S. Yan, B. Tian, J. Zhang, M. Anpo, Preparation of TiO2–SiO2 film with high photocatalytic activity on PET substrate, Mater. Lett. 60 (3) (Feb. 2006) 396–399.
[23] J. Krýsa, M. Baudys, A. Mills, Quantum yield measurements for the photocatalytic oxidation of Acid Orange 7 (AO7) and reduction of 2,6-dichlorindophenol (DCIP) on transparent TiO2 films of various thickness, Catal. Today 7 (2-7) (May 2014).
[24] X. Gao, I.E. Wachs, Titania–silica as catalysts: molecular structural characteristics and physico-chemical properties, Catal. Today 51 (2) (Jun. 1999) 233–254.
[25] C. Anderson, A.J. Bard, An Improved Photocatalyst of TiO2/SiO2 Prepared by a Sol-Gel Synthesis, J. Phys. Chem. 99 (24) (Jun. 1995) 9882–9885.
[26] Furlong D. Neil, The Colloid Chemistry of Silica, vol. 234, American Chemical Society, Washington DC, 1994.
[27] N.S. Allen, M. Edge, A. Ortega, G. Sandoval, C.M. Liauw, J. Verran, J. Stratton, R.B. McIntyre, Degradation and stabilisation of polymers and coatings: Nano versus pigmentary titania particles, Polym. Degrad. Stab. 85 (2004) 927–946.
[28] D. Scalarone, M. Lazzari, O. Chiantore, Acrylic protective coatings modified with titanium dioxide nanoparticles: comparative study of stability under irradiation, Polym. Degrad. Stab. 97 (11) (2012) 2136–2142.
[29] J. Mo, Y. Zhang, Q. Xu, R. Yang, Effect of TiO2/adsorbent hybrid photocatalysts for toluene decomposition in gas phase, J. Hazard. Mater. 168 (2009) 276–281.
[30] M.-J. López-Muñoz, R. van Grieken, J. Aguado, J. Marugán, Role of the support on the activity of silica-supported TiO2 photocatalysts: structure of the TiO2/SBA-15 photocatalysts, Catal. Today 101 (3–4) (Apr. 2005) 307–314.
[31] K. Gude, V.M. Gun'ko, J.P. Blitz, Adsorption and photocatalytic decomposition of methylene blue on surface modified silica and silica-titania, Colloids Surf. A Physicochem. Eng. Asp. 325 (1-2) (Jul. 2008) 17–20.
[32] A. Tracton, Coatings Technology : Fundamentals, Testing, and Processing Techniques, CRC Press, Boca Raton FL, 2007.
[33] S. Bloss, L. Elfenthal, Doped Titanium Dioxide as a photocatalyst for UV and visible light, in: International RILEM symposium on Photocatalysis, Environment and Construction Materials, 2007, no. October, pp. 31–38.
[34] Q.L. Yu, M.M. Ballari, H.J.H. Brouwers, Indoor air purification using heterogeneous photocatalytic oxidation. Part II: kinetic study, Appl. Catal. B Environ. 99 (1–2) (Aug. 2010) 58–65.
[35] D.M. Murphy, D.W. Fahey, Mathematical treatment of the wall loss of a trace species in denuder and catalytic converter tubes, Anal. Chem. 59 (23) (Dec. 1987) 2753–2759.
[36] S. Ifang, M. Gallus, S. Liedtke, R. Kurtenbach, P. Wiesen, J. Kleffmann, Standardization methods for testing photo-catalytic air remediation materials: problems and solution, Atmos. Environ. 91 (Jul. 2014) 154–161.
[37] C. Minero, A. Bedini, M. Minella, On the standardization of the photocatalytic gas/solid tests, Int. J. Chem. React. Eng. (Jan. 2013) 1–16.
[38] X. Fu, L.A. Clark, Q. Yang, M.A. Anderson, Enhanced photocatalytic performance of titania-based binary metal oxides: TiO 2 /SiO 2 and TiO 2 /ZrO 2, Environ. Sci. Technol. 30 (2) (Jan. 1996) 647–653.
[39] E. Rahmani, A. Ahmadpour, M. Zebarjad, Enhancing the photocatalytic activity of TiO2 nanocrystalline thin film by doping with SiO2, Chem. Eng. J. 174 (2-3) (Nov. 2011) 709–713.
[40] Y. Ohko, Y. Nakamura, A. Fukuda, S. Matsuzawa, K. Takeuchi, Photocatalytic Oxidation of Nitrogen Dioxide with TiO 2 Thin Films under Continuous UV-Light Illumination, J. Phys. Chem. C 112 (28) (Jul. 2008) 10502–10508.
[41] K. Guan, Relationship between photocatalytic activity, hydrophilicity and self-cleaning effect of TiO2/SiO2 films, Surf. Coat. Technol. 191 (2–3) (Feb. 2005) 155–160.
[42] Y. Li, S.-J. Kim, Synthesis and characterization of Nano titania particles embedded in mesoporous silica with both high photocatalytic activity and adsorption capability, J. Phys. Chem. B 109 (25) (Jun. 2005) 12309–12315.
[43] J. Krýsa, M. Baudys, M. Zlámal, H. Krýsová, M. Morozová, P. Klusoň, Photocatalytic and photoelectrochemical properties of sol–gel TiO2 films of controlled thickness and porosity, Catal. Today 230 (Jul. 2014) 2–7.
[44] J. Zhang, B. Li, C. Han, J. Liu, One-pot synthesis of foamed titania–silica composite and its photocatalytic performance, Mater. Lett. 129 (Aug. 2014) 50–53.
[45] Y. Yao, N. Zhao, J. Feng, M. Yao, F. Li, Photocatalytic activities of Ce or Co doped nanocrystalline TiO2–SiO2 composite films, Ceram. Int. 39 (4) (May 2013) 4735–4738.